J. Fluid Mech. (1998), *vol.* 366, *pp.* 87–108. Printed in the United Kingdom

Lagrangian accelerations in geostrophic turbulence

By BACH LIEN HUA[1], JAMES C. McWILLIAMS[2] AND PATRICE KLEIN[1]

[1] Laboratoire de Physique des Oceans, IFREMER, BP 70, 29280 Plouzané, France
[2] Department of Atmospheric Sciences, UCLA Los Angeles, CA 90024, USA

(Received 15 September 1997 and in revised form 6 January 1998)

A distinctive property of Lagrangian accelerations in geostrophic turbulence is that they are governed by the large and intermediate scales of the flow, both in time and space, so that the inertial part of the dynamics plays a much larger role than in three-dimensional turbulence where viscous effects are stronger. For the case of geostrophic turbulence on a β-plane, three terms contribute to the Lagrangian accelerations: the ageostrophic pressure gradient which often is the largest term, a meridional acceleration due to the β-effect, and an acceleration due to horizontally divergent ageostrophic motions. Both their spectral characteristics and patterns in physical space are studied in this paper. In particular the total accelerations field has an inertial spectrum slope which is identical to the geostrophic velocity field inertial slope.

The accelerations gradient tensor is shown to govern the topology of quasi-geostrophic stirring and transport properties. Its positive eigenvalues locate accurately the position of extrema of potential vorticity gradients. The three-dimensional distribution of tracer gradients is such that the vertical distribution is entirely constrained by the horizontal one, while the reverse is not true. We make explicit analytically their dependence on the three-dimensional accelerations gradient.

1. Introduction

This study addresses the characteristics of the Lagrangian accelerations in anisotropic (nearly horizontal) flows, motivated by the property of two-dimensional turbulent flows that their Lagrangian accelerations are mostly determined by the large and intermediate scales of motion, both in time and in space. Viscous effects thus play no significant role in these aspects of the dynamics. Lagrangian accelerations control the spatially local topology of tracer transport and the global statistics of turbulent dispersion.

For stationary two-dimensional turbulence, the Lagrangian velocity correlation function is $R(\tau) = \frac{1}{2}E\langle \boldsymbol{u}(t)\cdot\boldsymbol{u}(t+\tau)\rangle$, where $\langle\ \rangle$ designates time and ensemble mean over particle trajectories, with $2E = \langle|\boldsymbol{u}|^2\rangle$ and $\boldsymbol{u} = (u, v)$. The Lagrangian microscale T_m and integral time scale T_L (Taylor 1921) are defined as

$$T_m^{-2} = -\tfrac{1}{2}\mathrm{d}^2R/\mathrm{d}\tau^2 = \tfrac{1}{4}E\langle|\mathrm{d}\boldsymbol{u}/\mathrm{d}t|^2\rangle,$$

$$T_L = \int_0^\infty R(\tau)\mathrm{d}\tau.$$

T_m is therefore related to the mean square of the Lagrangian acceleration, $\boldsymbol{\gamma}_L = \mathrm{d}\boldsymbol{u}/\mathrm{d}t$, and the global diffusion coefficient is $K = 2E\,T_L$, provided the integral defining T_L converges. For two-dimensional inviscid dynamics, an approximate relation between T_m and T_L must exist since enstrophy conservation implies that the dynamics is characterized by a single time scale (Babiano *et al.* 1987). The Lagrangian velocity frequency spectrum normalized by the energy, $S(\nu)$ where ν is the frequency, is the Fourier transform of the correlation function $R(\tau)$. The micro- and integral time scales can be re-expressed as

$$T_m^{-2} = 4\pi^2 \int_0^\infty S(\nu)\nu^2 \mathrm{d}\nu,$$
$$T_L = \tfrac{1}{2}S(0).$$

Thus the micro-time scale is well defined only if the Lagrangian velocity frequency spectrum decreases faster than ν^{-3} at large ν, such that the variance of the Lagrangian accelerations will be finite. Furthermore T_m will be independent of Reynolds number if this spectrum decrease occurs by inertial dynamics. The ratio $\alpha = T_L/T_m$ depends upon the specific shape of $S(\nu)$ and is of order unity if $S(\nu)$ falls steeply enough.

The key point is that the steepness of the Lagrangian velocity spectrum for two-dimensional dynamics leads to a proportionality between the inverse square of the Lagrangian integral time scale and the variance of Lagrangian acceleration,

$$T_L^{-2} = \alpha^{-2}\frac{1}{4E}\langle|\boldsymbol{\gamma}_L|^2\rangle, \tag{1.1}$$

where the constant α is of order unity for flow regimes of a moderately anisotropic turbulence (i.e. precluding persistent jets).

Examples of Lagrangian velocity spectra observed in oceanic data and obtained in numerical simulations of strong geostrophic turbulence on a β-plane are shown in figure 1 (Rupolo *et al.* 1996). They confirm two characteristic features. The first feature is the existence of a plateau-like shape at the lowest frequencies near $\nu = 0$ so that T_L is well-defined. The second and most relevant feature for the present study is the steep decrease at high frequencies $S(\nu) \propto \nu^{-p}$ with $p > 3$, so that T_m is well-defined†. The computed values for α are 0.86 for the oceanic data and 1.06 for the numerical simulation of figure 1.

The steepness of the Lagrangian velocity spectrum found in the numerical simulations implies that Lagrangian accelerations exhibit no significant viscous effects and are governed by low and intermediate frequencies. These results differ markedly from those of three-dimensional turbulence, where numerous studies of pressure-gradient fluctuations have been conducted since the original investigation of Taylor (1935), in order to determine the non-viscous part of the Lagrangian accelerations. For high enough Reynolds numbers, the pressure field was originally thought to be closely related to the dispersion of marked particles, e.g. Batchelor (1951). However, in three-dimensional turbulence the decorrelation of the pressure gradient field takes place at much smaller separation distances than for the velocity field, and is mainly determined by the smallest-scale disturbances (Borgas & Sawford 1991).

† The value of p is ≈ 5.3 for the numerical simulation (dotted line), while it is ≈ 3.3 for the narrower frequency range resolved by the oceanic data of figure 1 (continuous line); no effort has been made to match the simulation to the observational context, although we note that the slope p is ≈ 4.3 for the numerical simulation if we restrict the fit to the same range of frequencies as those resolved in the oceanic data (see also Babiano, Basdevant & Sadourny 1985).

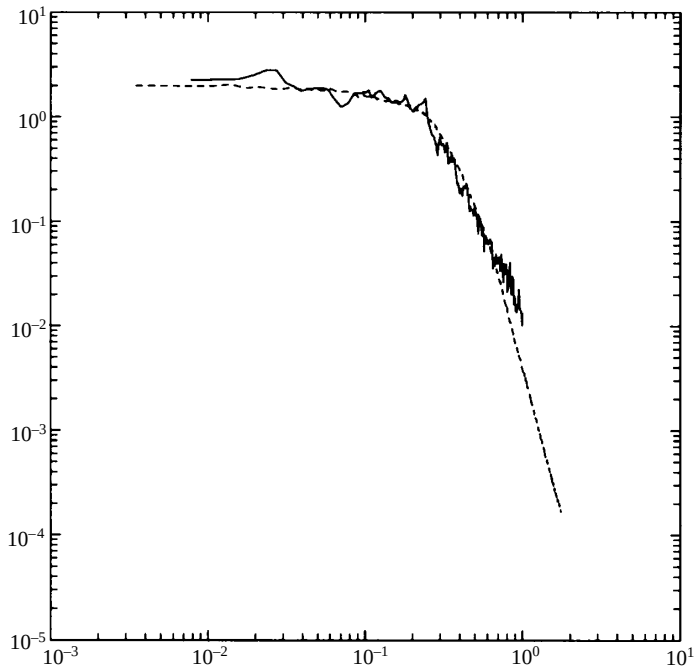

FIGURE 1. Normalized Lagrangian velocity frequency spectra from oceanic data (continuous line) and from a numerical simulation on the β-plane (dotted line) for turbulence forced by the baroclinic instability of a mean vertical shear (see §4). The abscissa corresponds to non-dimensional frequency νT_L and the ordinate is in units of T_L.

An important issue in the problem of turbulent transport in the presence of coherent structures is how to partition the fluid into regions with different dynamical properties (e.g. Elhmaïdi, Provenzale & Babiano 1994). For the physical-space characteristics, the Lagrangian accelerations of two-dimensional flows have been shown to govern the topology of turbulent transport of scalars. More specifically, the eigenvalues of the Lagrangian accelerations gradient tensor provide a criterion for partitioning the flow into regions with different stirring characteristics (Hua & Klein 1997), where stirring is defined as the growth of scalar gradients. This work also points out the central role played by the pressure field in the stirring problem, as already noted by Basdevant & Philipovitch (1994).

A purpose of the present study is the generalization of the two-dimensional results about the properties of transport in physical space to the regime of horizontally homogeneous geostrophic turbulence. This regime is more relevant to oceanic observations, by taking into account the effects of a stable density stratification S and planetary rotation with a meridional gradient in the Coriolis frequency β. The implication of the density stratification for geostrophic turbulence has been studied by Charney (1971), Rhines (1979), Herring (1980), Hua & Haidvogel (1986), McWilliams (1989), and McWilliams, Weiss & Yavneh (1994). The role of the β-effect in geostrophic turbulence has thus far only been addressed in two-dimensional and shallow-water flows. This was originally analysed by Rhines (1975), and more recent research on the β-plane or on the sphere (Maltrud & Vallis 1991; Cho & Polvani 1996) has confirmed the possibility of several different flow regimes for balanced dynamics. Strongly turbulent regimes can exist without excessive levels of anisotropy, and the β-effect

is known to curb considerably the spatial intermittency of the Eulerian fields when compared to the f-plane case (McWilliams 1984; Holloway 1986). These moderately anisotropic, strongly turbulent regimes on a β-plane are addressed in the present work for fully baroclinic quasi-geostrophic flows. We here will avoid flow regimes with a strong anisotropy associated with persistent zonal jets (Bartello & Holloway 1991; Panetta 1993), which do not seem relevant for the northwestern Atlantic where the oceanic data analysed in Rupolo *et al.* (1996) originate. We also leave aside the strongly intermittent regime dominated by coherent vortices when $\beta = 0$ (McWilliams *et al.* 1994).

The questions we address are (i) how different from the purely two-dimensional regime is the quasi-geostrophic transport behaviour, and (ii) which dynamical degrees of freedom govern the Lagrangian acceleration?

Since Lagrangian accelerations shape the topology of horizontal stirring locally in physical space (Hua & Klein 1997), we first evaluate in §2 the degrees of freedom governing the Lagrangian accelerations of quasi-geostrophic motions. Such dynamics allow a variation of the primary geostrophic horizontal velocity field in the vertical direction, and this raises the issue of comparing the quasi-geostrophic transport properties with those of the two- and three-dimensional cases. We derive in particular the criterion which should govern the topology of quasi-geostrophic stirring. Numerical diagnosis of the components of the Lagrangian accelerations is made in §3; they are found to agree reasonably well with the analytical results derived in the Appendix based on the Eulerian wavenumber spectra and a quasi-normal statistical hypothesis. Moreover, the spatial distribution of potential vorticity gradients found in the numerical simulations is compared with the analytical criterion for quasi-geostrophic stirring of §3. Finally, §4 summarizes the conclusions.

2. Quasi-geostrophic Lagrangian accelerations components

The approach follows closely the strictly two-dimensional treatment of Hua & Klein (1997) by evaluating the quasi-geostrophic Lagrangian accelerations. For that purpose, we need approximations of the momentum equations which are compatible with quasi-geostrophy.

2.1. *Momentum equations*

The formalism is introduced here for the case of a stratified fluid rotating at a rate of $\Omega = f(y)/2 = (f_0 + \beta\, y)/2$, where y designates the meridional direction coordinate. Quasi-geostrophy theory is based on an expansion in Rossby number $\mathscr{R} = U/fL \ll 1$ for all variables (Pedlosky 1987), where U and L are characteristic velocity and length scales. We truncate at first order the horizontal velocity $\boldsymbol{u} = (u, v)$, vertical velocity w and pressure field p:

$$(\boldsymbol{u}, w, p) = (\boldsymbol{u}_0 + \mathscr{R}\boldsymbol{u}_1, \quad w_0 + \mathscr{R}w_1, \quad p_0 + \mathscr{R}p_1).$$

In the following, the symbols ∇ and $\Delta = \nabla^2$ only denote horizontal operators. At zeroth order, the velocity field is purely geostrophic and strictly horizontal with

$$\boldsymbol{u}_0 = \frac{1}{\rho f_0}\boldsymbol{k} \times \nabla p_0, \quad w_0 = 0,$$

where $\boldsymbol{k}$ is the vertical unit vector and ρ is the mean background density. The dependence of this primary flow upon the vertical coordinate z is simply parametric,

and depth variations of the horizontal velocity field are mediated through the z-dependence of the geostrophic streamfunction, $\psi_0 = p_0/\rho f_0$, such that $\boldsymbol{u}_0 = \boldsymbol{k} \times \nabla\psi_0(x, y, z, t)$.

A general property of quasi-geostrophy is that it is an asymptotic theory in which once the geostrophic streamfunction ψ_0 (or p_0) is known, then all other quantities are known in principle; that is, given ψ_0 there are diagnositic relations for all other quantities that involve at most the inversion of spatial differential operators. Our primary point here is that certain Lagrangian quantities are most directly related to the ageostrophic Eulerian fields, and in particular the flow field can evolve with time only via these 'hidden' $O(\mathscr{R})$ dynamics, so that it is worth dealing with them explicitly.

We assume that the non-divergent geostrophic flow is entirely absorbed at $O(1)$, hence the $O(\mathscr{R})$ dynamics need only contain the divergent part of the flow and the ageostrophic pressure. The ageostrophic velocity field is defined by a divergence potential χ_1 such that

$$\boldsymbol{u}_1 = \nabla\chi_1, \quad \frac{\partial w_1}{\partial z} = -\Delta\chi_1.$$

The ageostrophic vertical velocity w_1 is related to the displacements of density isosurfaces

$$f_0\, S w_1 = -\frac{\mathrm{d}_g}{\mathrm{d}t}(\partial_z \psi_0), \tag{2.1}$$

where the operator $\mathrm{d}_g/\mathrm{d}t = \partial/\partial t + (\boldsymbol{u}_0 \cdot \nabla)$ denotes the geostrophic total derivative and S is the mean stratification parameter. The horizontal Lagrangian accelerations $\boldsymbol{\gamma}_L$, which also vary parametrically with z, are

$$\boldsymbol{\gamma}_L = \frac{\mathrm{d}_g \boldsymbol{u}_0}{\mathrm{d}t} = -\nabla p_1 - f_0\, \boldsymbol{k} \times \nabla\chi_1 + \beta y \nabla\psi_0, \tag{2.2}$$

where viscous effects are neglected. The quasi-geostrophic accelerations are induced by the ageostrophic circulation which involves both the pressure field p_1 and the three-dimensional velocity field ($\boldsymbol{u}_1$, w_1). An additional term is furthermore induced by differential rotation ($\beta \neq 0$). Comparing (2.2) with the non-rotating two-dimensional Euler equations in which the gradient of the pressure field p_1 totally determines the Lagrangian accelerations, we see that there are additional terms due to the Coriolis force induced by the horizontally divergent velocity field $\boldsymbol{u}_1$ and to the β-effect.

Differential rotation effects raise two issues: (i) the inherent anisotropy between the zonal and meridional direction; (ii) the consistency of a homogeneous representation of the dynamics in the meridional direction. The first issue is of less concern here, since we focus on isotropic scalar measures, such as the variance of Lagrangian acceleration, and leave for future work the introduction of an anisotropic tensorial representation such as used in McWilliams *et al.* (1986). For the second issue, we use periodic lateral boundary conditions as a simple depiction of horizontal homogeneity. Mathematical consistency requires that we consider only partial differential equations with spatially periodic coefficients, yet the Coriolis frequency $f(y)$ is non-periodic. However the quasi-geostrophic potential vorticity equation is well-known to have spatially uniform coefficients, hence horizontal periodicity for ψ_0 and $\boldsymbol{u}_0$ is allowed. It turns out that the Lagrangian accelerations $\boldsymbol{\gamma}_L$ can also be periodic on the β-plane as seen by rewriting (2.2) as

$$\boldsymbol{\gamma}_L = -\nabla\hat{p}_1 - \beta\psi_0 \boldsymbol{j} - f_0 \boldsymbol{k} \times \nabla\chi_1, \tag{2.3}$$

where $\boldsymbol{j}$ is the unit vector in the meridional direction and with the new variable

$$\hat{p}_1 = p_1 - \beta y \psi_0.$$

Besides the periodic field ψ_0, the right-hand side of (2.3) involves the two fields $\widehat{p}_1$ and χ_1 for which horizontal periodicity can also be appropriate as we shall now show by examining their diagnostic equations.

2.2. *Diagnostic equations for accelerations components*

The diagnostic equation for $\hat{p}_1$ is obtained by taking the horizontal divergence of (2.3),

$$\nabla^2 \hat{p}_1 = 2J_{xy}(u_0, v_0) + \beta u_0. \tag{2.4}$$

The right-hand side contains no polynomial dependence in y and only involves the components of the periodic velocity field $\boldsymbol{u}_0$, so that $\hat{p}_1$ can be periodic.

The curl of (2.3) yields the usual quasi-geostrophic potential vorticity equation

$$\frac{\mathrm{d}_g}{\mathrm{d}t} q + \beta \partial_x \psi_0 = 0, \quad q = \left(\nabla^2 + \partial_z \frac{1}{S} \partial_z \right) \psi_0. \tag{2.5}$$

The diagnostic equation for χ_1 is obtained by eliminating the time derivative from the density and potential vorticity equations, (2.1) and (2.5), leading to

$$\left.\begin{aligned} \left(\nabla^2 + \partial_z \frac{1}{S} \partial_z \right) (f_0 \nabla^2 \chi_1) &= -2\partial_z \frac{1}{S} \nabla \cdot \boldsymbol{Q} - \beta \partial_z \frac{1}{S} \partial_z v_0, \\ \boldsymbol{Q} &= -J_{xy}(\nabla \psi_0, \partial_z \psi_0), \end{aligned}\right\} \tag{2.6}$$

where the vector $\boldsymbol{Q}$ of Hoskins, Draghici & Davies (1978) has been introduced. The right-hand side of (2.6) again does not contain any polynomial dependence and only involves periodic functions, so that χ_1 can also be spatially periodic.

The fields $\hat{p}_1$, ψ_0 and χ_1 being periodic, the Lagrangian accelerations defined by (2.3) are also periodic. The presence of the β-term causes many important behaviours such as suppression of zonal gradients, westward phase propagation, and northwestward [southwestward] acceleration of cyclonic [anticyclonic] vortices, but it does not prevent the meridional periodicity of the Lagrangian acceleration.

2.3. *A criterion for quasi-geostrophic stirring*

A Taylor expansion for the leading-order quasi-geostrophic accelerations of fluid particles locally in physical space, just as in the two-dimensional case (Hua & Klein, 1997), leads to

$$\begin{pmatrix} \ddot{x} \\ \ddot{y} \\ \ddot{z} \end{pmatrix} = \boldsymbol{B} \begin{pmatrix} x \\ y \\ z \end{pmatrix} + \begin{pmatrix} \gamma_x(0) \\ \gamma_y(0) \\ 0 \end{pmatrix}, \tag{2.7}$$

with a (3×3) accelerations gradient tensor

$$\boldsymbol{B} = \begin{bmatrix} \partial_x \gamma_x & \partial_y \gamma_x & \partial_z \gamma_x \\ \partial_x \gamma_y & \partial_y \gamma_y & \partial_z \gamma_y \\ 0 & 0 & 0 \end{bmatrix}, \tag{2.8}$$

where $\boldsymbol{\gamma}_L = (\gamma_x, \gamma_y)$ and the dot symbol denotes the time derivative following the geostrophic flow, $\mathrm{d}_g/\mathrm{d}t$. The vertical component of acceleration is identically zero because of the hydrostatic assumption underlying quasi-geostrophic dynamics. A restriction of (2.8) to the case of motions which lie strictly in vertical planes, such as

(x, z) or (y, z), leads to degenerate dynamics of particle stirring at leading order, but the stirring problem is non-trivial in a horizontal plane (x, y) at a given vertical level z. In that case, one finds

$$\nabla\boldsymbol{\gamma}_L = -[\hat{p}_1''] - \boldsymbol{I}[f_0\chi_1''] - \beta \begin{bmatrix} 0 & 0 \\ \partial_x\psi_0 & \partial_y\psi_0 \end{bmatrix}, \tag{2.9}$$

where $\boldsymbol{I}$ is the rotation matrix of $\pi/2$ in the horizontal plane

$$\boldsymbol{I} = \begin{bmatrix} 0 & -1 \\ 1 & 0 \end{bmatrix}.$$

When compared to the strictly two-dimensional case (Hua & Klein 1998), besides the Hessian matrices of $\hat{p}_1$, the accelerations gradient tensor (2.9) involves two additional terms: the rotated Hessian matrix of χ_1 and a term due to the β-effect. Its eigenvalues, which govern the quasi-geostrophic stirring at a given level z, are given by

$$\lambda_\pm = \tfrac{1}{4}W \pm \tfrac{1}{2}(\dot{\sigma}_n^2 + \dot{\sigma}_s^2 - \dot{\omega}^2)^{1/2}, \tag{2.10}$$

and the vorticity ω and the normal and shear strain rates, σ_n, σ_s, (e.g. Kundu 1990, p. 56) are

$$\begin{aligned} \omega &= \partial_x v_0 - \partial_y u_0 = (\partial_{xx} + \partial_{yy})\psi_0, \\ \sigma_n &= \partial_x u_0 - \partial_y v_0 = -2\partial_{xy}\psi_0, \\ \sigma_s &= \partial_x v_0 + \partial_y u_0 = (\partial_{xx} - \partial_{yy})\psi_0. \end{aligned}$$

More specifically, terms involved in the eigenvalues are

$$\left.\begin{aligned} \dot{\sigma}_n &= -(\partial_{xx} - \partial_{yy})\hat{p}_1 + 2\partial_{xy}f_0\chi_1 - \beta u_0, \\ \dot{\sigma}_s &= -2\partial_{xy}\hat{p}_1 - (\partial_{xx} - \partial_{yy})f_0\chi_1 - \beta v_0, \\ \dot{\omega} &= -(\partial_{xx} + \partial_{yy})f_0\chi_1 - \beta v_0, \\ \tfrac{1}{2}W &= -(\partial_{xx} + \partial_{yy})\hat{p}_1 + \beta u_0, \end{aligned}\right\} \tag{2.11}$$

thereby involving both $\hat{p}_1$, χ_1 and β. The quantities $\dot{\sigma}_s$, $\dot{\sigma}_n$ and $\dot{\omega}$ in (2.11) are readily evaluated by spatial differentiation of the accelerations $\dot{u}_0$ and $\dot{v}_0$. This enables the physical interpretation of the radicand, which in practice is computed from the components of the pressure Hessian matrices of $\hat{p}_1$, χ_1. Moreover, (2.11) emphasizes the important role played by the anisotropy between the zonal and meridional directions in the fields $\widehat{p}_1$, χ_1, and also induced by the β-effect, for modifying the strain components along a particle trajectory.

These Lagrangian variations of the strain components are quantitatively important, and in both the two-dimensional and quasi-geostrophic cases, the topology of stirring is governed by $\lambda_\pm$, which is better than the approximate Okubo–Weiss criterion

$$\lambda_0 = \tfrac{1}{4}W = \tfrac{1}{4}(\sigma^2 - \omega^2) = -J_{xy}(\partial_x\psi, \partial_y\psi), \quad \sigma^2 = \sigma_n^2 + \sigma_s^2, \tag{2.12}$$

where J_{xy} denotes the Jacobian operator with respect to the coordinates x, y. The criterion λ_0 is obtained by neglecting the radicand in (2.10), through an assumption of slowly evolving fields (Okubo 1970; Weiss 1991). It has been widely used to diagnose different dynamical properties of the flow in numerical simulations (McWilliams 1984; Benzi, Patarnello & Santangelo 1988; Brachet *et al.* 1988; Elhmaïdi *et al.* 1994). However, Basdevant & Philipovitch (1994) have provided numerical evidence that the validity of the assumption of slowly evolving fields is restricted either to the centre of the vortex cores or to the immediate vicinity of the saddle points of ψ_0. Hua & Klein (1998) have shown that, outside the vortex cores, the

positive values of λ_+ can be three times larger than those of λ_0 because of the dominance of $\dot{\sigma}_s$ and $\dot{\sigma}_n$. Furthermore, these Lagrangian variations of the strain are associated with large spatial scales which are far-reaching outside the vortex cores (Hua & Klein 1998), and this is mediated through the non-local interactions associated with the pressure for an incompressible fluid (Ohkitani & Kishiba 1995).

The ageostrophic pressure field $\hat{p}_1$ has been found in Hua & Klein (1998) to be the key quantity, and the role of λ_0 is merely to force its patterns, since λ_0 appears in the right-hand side of the diagnostic equation (2.4) for $\hat{p}_1$. λ_0 can be interpreted as being *the generalized centrifugal force divergence*, since it corresponds to the divergence of the horizontal accelerations. From (2.12), we can also recognize λ_0 as proportional to the nonlinear correction to the geostrophic balance that makes the gradient-wind balance relation such an accurate approximation for slowly evolving, large-scale motions in the ocean and atmosphere. It is therefore akin to the Lighthill theory of sound generation from a turbulent source (Lighthill 1978). The quadrupole geometry which is forced by Lighthill's source term in the case of an isolated vortex prevails also in some regions of the numerical results for $\widehat{p}_1$ reported in §3: this is because λ_0 implies second derivatives of ψ_0 through the Hessian determinant of the streamfunction:

$$-\lambda_0 = \begin{vmatrix} \partial_{xx}\psi_0 & \partial_{xy}\psi_0 \\ \partial_{xx}\psi_0 & \partial_{yy}\psi_0 \end{vmatrix} = \left|\psi_0''\right|. \tag{2.13}$$

We have thus generalized to the quasi-geostrophic case the evidence of the central roles played by the Hessian matrices of the pressure field ($\widehat{p}_1$) and of the divergence potential χ_1, and $\beta\nabla\psi_0$ as shown by (2.9), instead of merely λ_0, the determinant of the Hessian of the streamfunction field ψ_0.

2.4. *Three-dimensional topology of stirring and distribution of tracer gradients*

Quasi-geostrophic stirring is entirely described by $\hat{p}_1$, χ_1 and the β-effect term. The $\hat{p}_1$ and χ_1 fields have depth variations which are not independent, since both fields determine the three-dimensional ageostrophic circulation necessary to maintain the instantaneous thermal wind balance of the zeroth-order flow (Davies-Jones 1991). Their depth variations cause in turn those of the quasi-geostrophic stirring through (2.10) and (2.11). However, as a consequence of the degenerate character of the (3×3) accelerations gradient tensor $\boldsymbol{B}$ defined in (2.8), the vertical distribution of stirring properties is strongly constrained by the horizontal distribution, as will be elaborated below.

Denoting by $\theta(x, y, z)$ a tracer field such that

$$\frac{\mathrm{d}_g}{\mathrm{d}t}\theta = 0,$$

the three-dimensional tracer gradient equation can be written

$$\frac{\mathrm{d}_g^2}{\mathrm{d}t^2}\nabla_3\theta = \boldsymbol{M}\nabla_3\theta, \tag{2.14}$$

where the ∇_3 operator is $\nabla_3 = (\partial_x,\ \partial_y,\ \partial_z)$. One expects that the properties of the matrix $\boldsymbol{M}$ govern the spatial distribution of the tracer gradient. $\boldsymbol{M}$ is related to both

the velocity gradient tensor

$$\boldsymbol{A} = \begin{bmatrix} \partial_x u_0 & \partial_y u_0 & \partial_z u_0 \\ \partial_x v_0 & \partial_y v_0 & \partial_z v_0 \\ 0 & 0 & 0 \end{bmatrix}$$

and the (3×3) accelerations gradient tensor $\boldsymbol{B}$ through

$$\boldsymbol{M} = 2\boldsymbol{A}^{*2} - \boldsymbol{B}^{*} = 2 \begin{bmatrix} -J_{xy}(u_0, v_0) & 0 & 0 \\ 0 & -J_{xy}(u_0, v_0) & 0 \\ J_{yz}(u_0, v_0) & J_{zx}(u_0, v_0) & 0 \end{bmatrix} - \begin{bmatrix} \partial_x \gamma_x & \partial_x \gamma_y & 0 \\ \partial_y \gamma_x & \partial_y \gamma_y & 0 \\ \partial_z \gamma_x & \partial_z \gamma_y & 0 \end{bmatrix}, \quad (2.15)$$

where the * symbol denotes the transpose of a tensor.

Using the relations between the Jacobian terms which appear in (2.15) with $\nabla \cdot \boldsymbol{\gamma}_L$ and $\boldsymbol{k} \cdot \nabla \times \boldsymbol{\gamma}_L$,

$$\left.\begin{aligned} -2J_{xy}(u_0, v_0) &= -\partial_x \left(\tfrac{\mathrm{d}_g}{\mathrm{d}t} \partial_y \psi_0\right) + \partial_y \left(\tfrac{\mathrm{d}_g}{\mathrm{d}t} \partial_x \psi_0\right) = \partial_x \gamma_x + \partial_y \gamma_y \\ &= \nabla \cdot \boldsymbol{\gamma}_L, \\ -2J_{yz}(u_0, v_0) &= \partial_z \left(\tfrac{\mathrm{d}_g}{\mathrm{d}t} \partial_y \psi_0\right) - \partial_y \left(\tfrac{\mathrm{d}_g}{\mathrm{d}t} \partial_z \psi_0\right) = -\partial_z \gamma_x - S f_0 \partial_y w_1 \\ &= -\partial_z \gamma_x - S \partial_y \left[\int (\boldsymbol{k} \cdot \nabla \times \boldsymbol{\gamma}_L + \beta v_0) \mathrm{d}z\right], \\ -2J_{zx}(u_0, v_0) &= -\partial_z \left(\tfrac{\mathrm{d}_g}{\mathrm{d}t} \partial_x \psi_0\right) + \partial_x \left(\tfrac{\mathrm{d}_g}{\mathrm{d}t} \partial_z \psi_0\right) = -\partial_z \gamma_y + S f_0 \partial_x w_1 \\ &= -\partial_z \gamma_y + S \partial_x \left[\int (\boldsymbol{k} \cdot \nabla \times \boldsymbol{\gamma}_L + \beta v_0) \mathrm{d}z\right], \end{aligned}\right\} \quad (2.16)$$

$\boldsymbol{M}$ can be expressed entirely in terms of accelerations gradient and of the β-effect through

$$\boldsymbol{M} = \begin{bmatrix} \partial_y \gamma_y & -\partial_x \gamma_y & 0 \\ -\partial_y \gamma_x & \partial_x \gamma_x & 0 \\ +S \partial_y \left[\int (\boldsymbol{k} \cdot \nabla \times \boldsymbol{\gamma}_L + \beta v_0) \mathrm{d}z\right] & -S \partial_x \left[\int (\boldsymbol{k} \cdot \nabla \times \boldsymbol{\gamma}_L + \beta v_0) \mathrm{d}z\right] & 0 \end{bmatrix}. \quad (2.17)$$

There have been numerous studies of the invariants of the velocity gradient tensor $\boldsymbol{A}$ in the literature, as a means to identify remarkable features of the turbulence, both in fully three-dimensional turbulence (e.g. Chong, Perry & Cantwell 1990) and also in two-dimensional turbulence (in that case, the Okubo–Weiss quantity is simply the double eigenvalue of $\boldsymbol{A}^2$). In contrast, we see here from (2.17) that $\boldsymbol{M}$ involves the accelerations gradient, and also the presence of the βv_0 term.

For the strictly two-dimensional case, the (2×2) matrix obtained from the first two columns and rows of $\boldsymbol{M}$ in (2.15), has the same eigenvalues as $[\nabla \boldsymbol{\gamma}_L]$ but with their relative order interchanged (Hua & Klein 1998). This corresponds to the usual result that in the spatial direction where particle separation increases most rapidly (positive values of λ_+), the tracer gradient will decrease in amplitude, and conversely, for the spatial direction for which particle separation decreases the most rapidly the tracer gradient amplitude will increase. These two-dimensional results are also valid for the quasi-geostrophic case at a given level z, and the $\lambda_\pm$ are expected to determine the horizontal distribution of tracer gradients. We shall test this conjecture

by comparing gradients of potential vorticity (which is an active tracer field whose distribution influences the velocity field) diagnosed in numerical simulations, with the quasi-geostrophic criterion for mixing provided by $\lambda_{\pm}$ in §3.

In the three-dimensional quasi-geostrophic case, equations (2.14) and (2.17) reveal that the variations along the z-coordinate of the distribution of tracer gradient are related to the horizontal tracer gradient. The vertical tracer gradient $\partial_z\theta$ is entirely determined by the horizontal gradient $\nabla\theta$, thereby making explicit the degenerate character of the vertical distribution of stirring properties,

$$\frac{\mathrm{d}_g^2}{\mathrm{d}t^2}\partial_z\theta = -S\boldsymbol{k}\cdot\left[\nabla\left(\int(\boldsymbol{k}\cdot\nabla\times\boldsymbol{\gamma}_L+\beta v_0)\mathrm{d}z\right)\times\nabla\theta\right]. \tag{2.18}$$

The reverse is not true, in that $\nabla\theta$ does not depend upon $\partial_z\theta$ (Klein, Tréguier & Hua 1998; Haynes & Anglade 1997).

Another approach for studying the three-dimensional distribution of properties in quasi-geostrophic flows has been based on the $\boldsymbol{C}$-vector introduced by Xu (1992). $\boldsymbol{C}$ is defined as the three-dimensional torque exerted upon the primary geostrophic flow by the secondary ageostrophic circulation,†

$$2\boldsymbol{C} = -\nabla_3\times\frac{\mathrm{d}_g}{\mathrm{d}t}\nabla_3\psi_0, \tag{2.19}$$

so that

$$\boldsymbol{C}\equiv(C_1,C_2,C_3) = -\big(J_{yz},\ J_{zx},\ J_{xy}\big)(u_0,v_0), \tag{2.20}$$

and its horizontal component ($\boldsymbol{C}_H=(C_1,C_2)=\boldsymbol{Q}\times\boldsymbol{k}$) and vertical one ($C_3=\lambda_0$) are respectively related to the $\boldsymbol{Q}$-vector and to the Okubo–Weiss criterion (Xu 1992). Equations (2.15) and (2.16) also make explicit the relations between the $\boldsymbol{C}$-vector and the components of $\boldsymbol{A}^{*2}$, as well as its expression in terms of $\nabla\cdot\boldsymbol{\gamma}_L$ and $\boldsymbol{k}\cdot\nabla\times\boldsymbol{\gamma}_L$.

However, the matrix $\boldsymbol{M}$, which we conjecture to determine the three-dimensional topology of tracer gradients, cannot be expressed simply in terms of the $\boldsymbol{C}$-vector and the role of the latter is in providing *the orientation of the Lagrangian rate of change* of the three-dimensional tracer gradient through

$$\boldsymbol{C}\cdot\frac{\mathrm{d}_g}{\mathrm{d}t}\nabla_3\theta = 0. \tag{2.21}$$

The last relation can be obtained from

$$\left.\begin{aligned}\frac{\mathrm{d}_g}{\mathrm{d}t}\nabla_3\theta &= -\boldsymbol{A}^*\nabla_3\theta,\\ C_1\partial_x u_0 + C_2\partial_y u_0 + C_3\partial_z u_0 &= 0,\\ C_1\partial_x v_0 + C_2\partial_y v_0 + C_3\partial_z v_0 &= 0.\end{aligned}\right\} \tag{2.22}$$

Thus in the same manner as the eigenvalue λ_0 differs from $\lambda_{\pm}$, the information contained in the $\boldsymbol{C}$-vector differs from that contained in $\boldsymbol{M}$: the set, λ_0 and $\boldsymbol{C}$, appears in a first order-in-time differential equation, e.g. (2.22), and involves the velocity gradient tensor $\boldsymbol{A}$, while the other set, $\lambda_{\pm}$ and $\boldsymbol{M}$, appears in a second order in time differential equation, e.g. (2.14), and involves the accelerations gradient tensor $\boldsymbol{B}=\nabla_3\boldsymbol{\gamma}_L$. Our main presumption is that the second-order-in-time equation is more likely to capture the topology of local turbulent transport properties, because it takes into account the variations in inertia along the Lagrangian particle trajectories, and more specifically the variations of the strain rate components.

† Our definition of $\boldsymbol{C}$ slightly differs from Xu (1992) by not including the β-term for simplification.

In summary, the main results of this section have been to motivate analytically the plausible importance of the accelerations gradient tensor in determining the topology of tracer gradients, and in documenting the differences expected between the properties of velocity gradient and accelerations gradient tensors for quasi-geostrophic flows.

3. Numerical diagnosis of accelerations components

Eulerian numerical simulations were performed with the spectral code reported in Hua & Haidvogel (1986, referred to as HH86 hereafter), solving the quasi-geostrophic potential vorticity equation (2.5) for a statistical equilibrium solution in the presence of forcing and damping. As in HH86 the forcing mechanism is provided by the baroclinic instability of a vertically sheared zonal mean flow $\overline{\psi}_0 = -\overline{u}_0(z)y$. Damping corresponds to a bottom friction through an Ekman layer and hyperviscosity is used as an enstrophy remover. Boundary conditions for the vertical structure are rigid lids at top ($z = 0$) and bottom ($z = -1$). The background stratification S corresponds to the exponential Brunt–Väisälä profile of HH86 (their figure 1*b*), which implies a zero-crossing of the first baroclinic mode around $z = -0.3$. The numerical simulations which are reported correspond to a resolution of 256^2 grid points in the horizontal, 8 layers in the vertical and the doubly periodic domain spans $7 \times 2\pi$ radii of deformation of the first baroclinic mode. The domain size is chosen as 2π in non-dimensional units and this sets the length scale, while the inverse time scale is set by the imposed mean vertical shear, and corresponds to typical midlatitude oceanic regimes as in HH86.

The numerical results are analysed both for the statistics at a given level z as well as the depth dependence of the components of the acceleration, $\hat{p}_1$, χ_1, and $\beta\psi_0$.

3.1. *Level-wise diagnostics*

Fields of ψ_0 and potential vorticity q are given in figures 2(*a*) and 2(*b*) at a given vertical level z, revealing marked frontal structures in the potential vorticity field, which tend to display an overall zonal orientation due to the β-effect.

Let us consider for a moment the case of geostrophic turbulence on an f-plane where differential rotation effects are neglected ($\beta = 0$). For horizontally homogeneous turbulence,

$$\langle \nabla p_1 \cdot (\boldsymbol{k} \times \nabla \chi_1) \rangle = 0, \tag{3.1}$$

where $\langle\ \rangle$ designates a horizontal spatial average. Consequently,

$$\langle |\boldsymbol{\gamma}_L|^2 \rangle = \langle |\nabla p_1|^2 \rangle + f_0^2 \langle |\nabla \chi_1|^2 \rangle, \tag{3.2}$$

and the variance of Lagrangian accelerations is the sum of two degrees of freedom which are spatially orthogonal and which come respectively from the ageostrophic pressure and divergence field.

Fields of ageostrophic $\hat{p}_1$ and χ_1 (with $\beta \neq 0$) are shown in figures 2(*c*) and 2(*d*). Locally organized structures can be identified in both fields, e.g. a quadrupole pattern is present in the upper left corner of both fields, with a rotation of nearly $\pi/2$ between the two quantities. (For $\beta = 0$, this angle is exactly $\pi/2$ as shown by (3.1).) Both the similarity of the spatial patterns and their relative angle are due to the phase relationship between the two quantities $\hat{p}_1$ and χ_1 which is implied by (3.1). Moreover, a tripole pattern is also present in the lower left corner of figure 2(*c*). In fact, quadrupole and tripole patterns correspond to what Lighthill (1978) calls lateral and longitudinal quadrupoles respectively. The former are forced by extra-diagonal terms of the second-derivative matrix in (2.13), while tripoles are forced by diagonal terms of

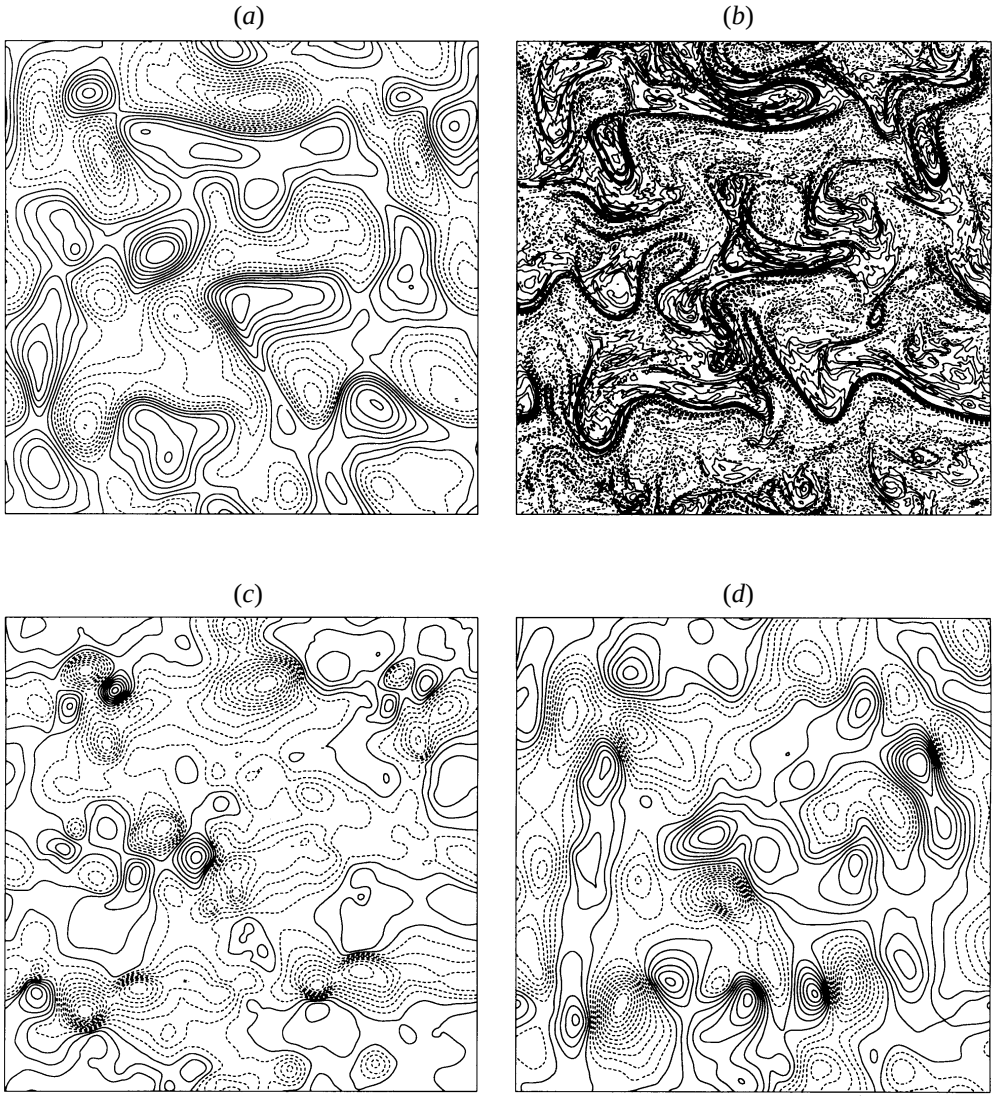

FIGURE 2. Fields of geostrophic streamfunction ψ_0 (*a*), potential vorticity q (*b*), ageostrophic pressure p_1 (*c*), and divergence potential χ_1 (*d*), at the top of the water column for an exponential stratification profile. Contour levels in non-dimensional units are respectively 0.2, 10, 2 and 1.

the matrix. Polvani *et al.* (1994) reported cases of dominance of dipoles caused by the mutual advection of elliptically deformed eddies in numerical simulations of shallow water with a finite radius of deformation, although we see fewer such structures in our quasi-geostrophic simulations; however, because they used a formalism for the wave generation equation that was one differential order higher in time than Lighthill's, a direct comparison of the source patterns is difficult, although we do not believe that our present results are qualitatively different on this issue.

A strong skewness is present in the pressure field, with positive areas of weaker amplitude than negative ones, the negative extremum being roughly twice the positive one. One can show that the skewness of the probability distribution of pressure is induced by the skewness of the distribution of W through (2.4). [Since W is a bilinear

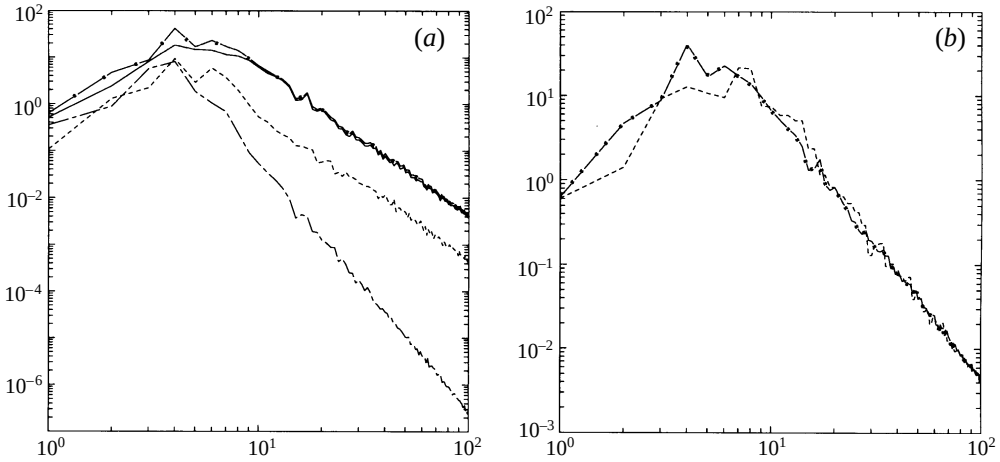

FIGURE 3. (*a*) Spectra of $|\nabla p|$ (continuous), $|\nabla\chi|$ (dotted line), $\beta\psi_0$ (long/short-dashed) and of $|\boldsymbol{\gamma}_L|$ (starred) at the top of the water column for a variable stratification profile. (*b*) Spectra of $|\boldsymbol{\gamma}_L|$ (starred) and of the analytical estimate (A8) (dotted)

quadratic form of vorticity and strain, it has an exponential, skewed distribution even in the case of a joint-normal distribution of the vorticity and strain components (Hua 1994). This skewness is due to differences in the geometry of the strain and vorticity fields, which are on average spatially orthogonal and have the same variance, yet strain posesses two degrees of freedom while vorticity has only one. In both two and three dimensions and also for quasi-geostrophic dynamics, the pressure field is diagnostically related to the distribution of strain and vorticity through (2.4) and that implies that the skewness in the probability distribution of W will carry over to the the probability distribution of pressure $\hat{p}_1$ (Holzer & Siggia 1993; Hua 1994)]. Values found for the skewness of $\hat{p}_1$ vary in time between -1 and -2, while the divergence potential χ_1 has a skewness which does not exceed -0.3 in the simulation of figure 2. We have performed a number of other numerical simulations varying both the stratification $S(z)$ and the forcing and sink amplitudes, and this marked discrepancy in the skewness of $\hat{p}_1$ and χ_1 is robust.

The spectra of the accelerations components $\nabla\hat{p}_1$, $\nabla\chi_1$, and $\beta\psi_0$ along with the total spectrum of $\boldsymbol{\gamma}_L$ are given in figure 3(*a*). The largest contribution by far in $|\boldsymbol{\gamma}_L|$ is due to the $\nabla\hat{p}_1$ term and its spectral characteristics are well-captured by the quasi-normal approximation (A 8) detailed in the Appendix which is also plotted in figure 3(*b*), which shows that the total accelerations field has an inertial spectrum slope which is identical to the geostrophic velocity field $|\boldsymbol{u}_0|$ inertial slope (for horizontal wavenumbers such that $k \geqslant 7$), consistently with (A 8). This result grants the property that the Lagrangian accelerations are governed by the large and intermediate spatial scales of the flow.

Moreover, the variance of the pressure gradient is given by (see Appendix)

$$\langle|\nabla\hat{p}_1|^2\rangle \approx \left(\tfrac{3}{4}Z(z) + 6\beta^2\frac{E(z)}{Z(z)}\right)E(z), \tag{3.3}$$

where E and Z designate respectively the kinetic energy and relative enstrophy at a given level z. The first term in (3.3) is the dominant one in the upper part of the water column for a solution with a moderate influence of the β-term (see the next subsection). Relation (3.3), when combined with (1.1), illustrates the considerably

shorter time scale, $(\langle|\nabla\hat{p}_1|^2\rangle/E)^{-1/2} \propto Z(z)^{-1/2}$, linked to a relative enstrophy time scale, which is associated with an immediate reorientation of structures under straining deformation effects. Such a time scale is much shorter than the advective time scale of the energy-containing eddy structures, $1/k_0E^{1/2}$, where k_0 is the wavenumber of the kinetic energy spectrum maximum. Relation (3.3), with β set to zero, is similar to the results of Babiano *et al.* (1987) and Larchevêque (1990) except for a constant factor of respectively 4 and 2 for the constant term multiplying Z in (3.3). The discrepancy arises because of the assumptions of Gaussian shapes for time and space covariances made by Babiano *et al.* and the closure-theory inertial-range spectrum assumption of k^{-3} made by Larchevêque.

3.2. *Local topology of stirring*

The purpose of this subsection is to test the topology of stirring as predicted, on the one hand by the positive values of the eigenvalues λ_+ and λ_0 defined in (2.10), with on the other hand the distribution of the gradient of the active tracer represented by potential vorticity q.

Figure 4 illustrates the comparison between these quantities at a given level z. The $|\nabla q|$ field is extremely filamentary and displays a tendency for zonal alignment, because of the β-effect. Extrema in gradients of potential vorticity have been studied as being dynamical barriers to transport and mixing (e.g. McIntyre 1989; Bowman & Chen 1994). We see on figure 4(b) that the locations of these extrema match well with those of the positive extrema of λ_+, and that almost all the main features of $|\nabla q|$ are also present in figure 4(b). On the other hand, the Okubo–Weiss criterion λ_0, positive values of which are shown on figure 4(c), matches less well with figure 4(a). The correlation between $|\nabla q|$ and positive λ_+ is 0.21, that between $|\nabla q|$ and positive λ_0 is 0.12 and that between $|\nabla q|$ and positive λ_- is $\leqslant 10^{-4}$. These values of the direct correlations, while favouring λ_+, are of weak magnitude. However if one correlates instead the areas of the regions where the various quantities are larger than a given threshold value (chosen as the contour intervals listed in the caption of figure 4), then the respective correlations are 0.70, 0.44 and 0.03. These results therefore support the statement that the properties of the accelerations gradient tensor – as diagnosed by λ_+ – capture more accurately the location in physical space of the high gradients of potential vorticity than the properties of the velocity gradient tensor – as diagnosed by λ_0.

The criteria λ_+ and λ_0 differ by the radicand term in (2.10) which involves the Lagrangian variation of the strain rate, and the above results confirm its quantitative importance in the topology of stirring. As pointed out by one of the referees, the Okubo–Weiss criterion λ_0 only takes into account the instantaneous strain, rather than the strain averaged along trajectories. The difference between figures 4(b) and 4(c) indicates that the strain in 4(c) is 'advected out' along trajectories, manifesting the non-local influence of $\dot{\sigma}_n$ and $\dot{\sigma}_s$ on tracer gradients. High gradients can thus be created by processing tracer through a small localized high-strain region, and our analytical approach is somewhat akin to a short-term trajectory calculation, where we solve the flow evolution equations by Taylor series, over a short time (see also Ohkitani & Kishiba 1995). The information which is obtained here with a completely diagnostic method could in principle also be obtained by computing short-term Lyapunov exponents (Pierrehumbert & Yang 1993), which do require however knowledge of the flow field at different time steps.

The tracer amplification problem at a given level z for the original (first order in Taylor series) problem involves $(\mathrm{d}_g/\mathrm{d}t)\nabla\theta$ and has two roots, while the second-order

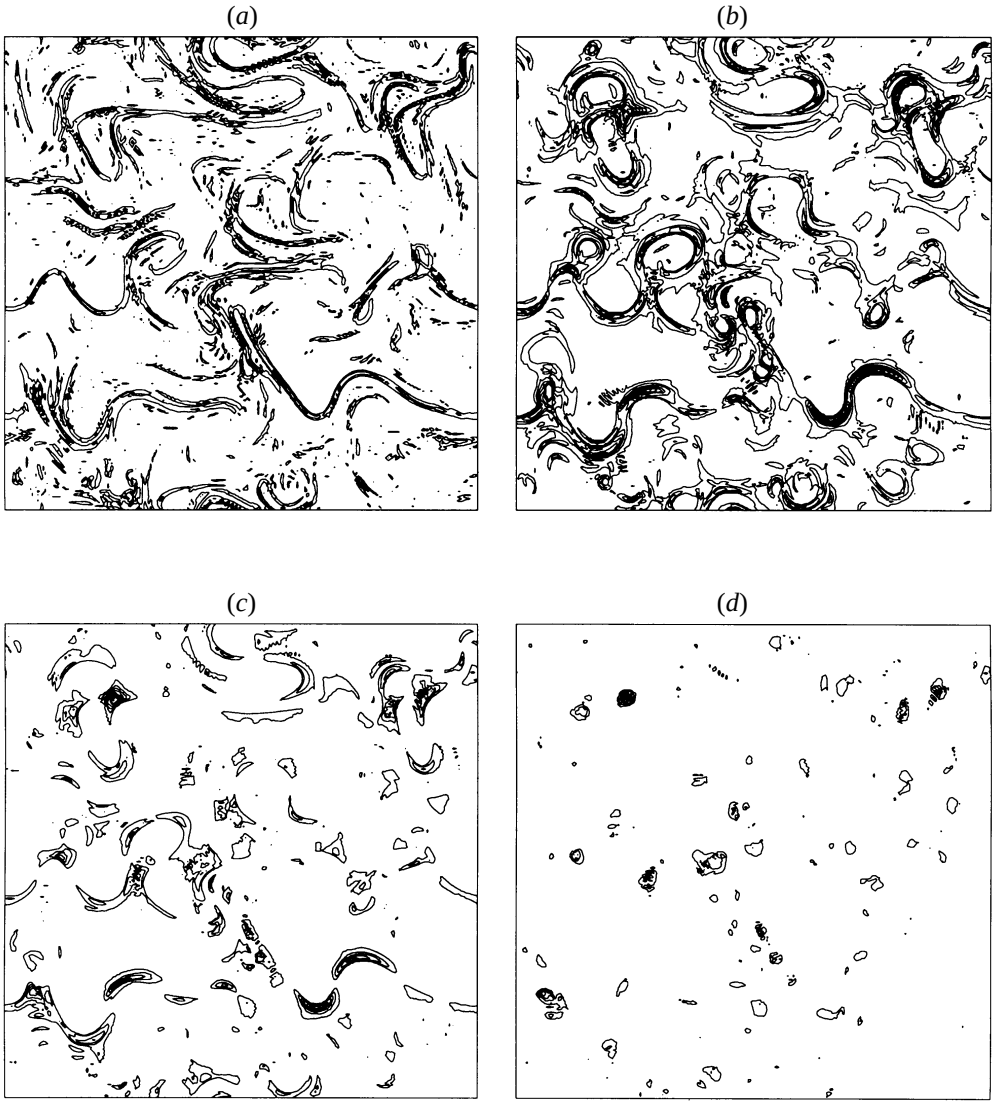

FIGURE 4. Fields of $|\nabla q|$ (*a*), and of the positive values of λ_+ (*b*), λ_0 (*c*), and λ_- (*d*), at the same level z as in figure 2. Contour levels in non-dimensional units are 650 for (*a*) and 150 for (*b–d*).

problem involving $(\mathrm{d}_g^2/\mathrm{d}t^2)\nabla\theta$ has four roots. The four initial scalar conditions which are needed in the latter case correspond to $\nabla\theta_{(t=0)}$ and $(\mathrm{d}_g/\mathrm{d}t)\nabla\theta_{(t=0)}$, where the last conditions are obtained by using the the first-order equation with $\nabla\theta_{(t=0)}$. Therefore only two independent initial conditions are sufficient for the two-dimensional advection problem at any order. Moreover, the tracer gradient $\nabla\theta$ at a given point is a linear combination of the appropriate set of eigenvectors for the problem under consideration. Basically, the largest positive eigenvalue is the relevant root if a growth of the tracer gradient is to be expected, and that root will dominate quantitatively if and only if the tracer gradient is nearly aligned with the associated eigenvector. The results of the numerical simulations suggest that high gradients of tracer match better with regions of high positive λ_+, and this implies that locally $\nabla\theta$ is nearly colinear to the λ_+ eigenvector. We are at present pursuing this line of investigation.

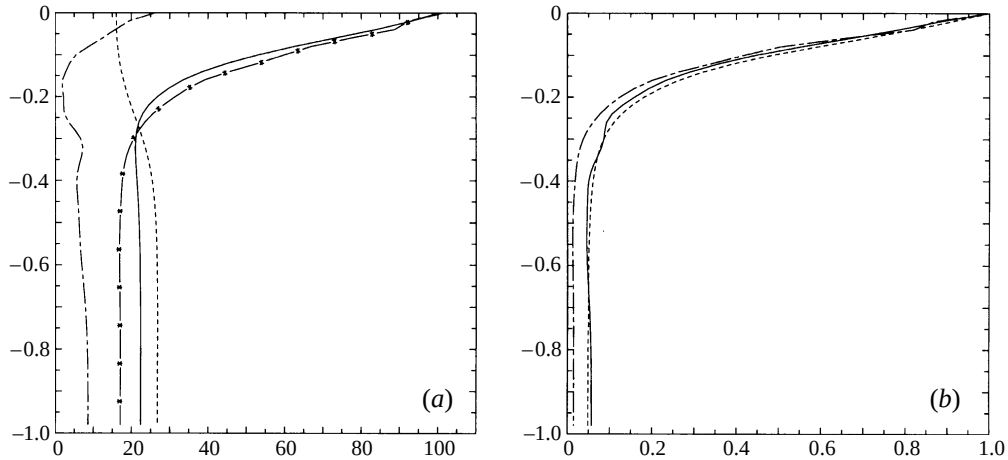

FIGURE 5. (*a*) Vertical profiles of the variance of the Lagrangian accelerations components: $\langle|\nabla p_1|^2\rangle/E$ (continuous line, numerical results; starred, analytical estimate (A5)), $\langle|\nabla\chi|^2\rangle/E$ (dash-dotted line), and $\langle|\beta\psi_0|^2\rangle/E$ (dotted). (*b*) Vertical profile of the total variance of the Lagrangian accelerations $\langle|\gamma_L|^2\rangle/E$ (continuous), $\langle q^2\rangle$ (dash-dotted) and E (dotted). All quantities in (*b*) are normalized by their value at $z = 0$.

We have diagnosed the various terms of (2.11) in the numerical simulations and found a robust overwhelming preponderance of the terms involving $\hat{p}_1$ over those involving either χ_1 or β, by at least a factor of 10. We therefore conclude that the role of β in the tracer transport, which is clearly seen through the tendency for zonal alignment in figure 4, is mediated indirectly through the influence of β on the characteristics of the ageostrophic pressure field $\hat{p}_1$ itself.

3.3. *Vertical structure*

The aim of this subsection is to document the vertical structure of the three components of accelerations (2.3), and results concerning the diagnosis of vertical tracer gradients will be reported elsewhere.

Figure 5(*a*) displays the vertical profiles of the variance of acceleration components. All our numerical simulations of forced turbulence present a strong dominance of the $|\nabla\hat{p}_1|$ component with respect to the other two in the upper part of the water column. We have overlayed on the same graph the analytical prediction for $|\nabla\hat{p}_1|^2$, given by (3.3), and we see a close correspondence with the numerical simulations. Except near the surface, $|\nabla\chi_1|^2$ remains small. The β-term presents a strong barotropic (nearly depth-independent) influence on the acceleration, and can become the dominant term below $z = -0.3$ as seen on figure 5(*a*).

While the analytical formula developed in the Appendix for $|\nabla\hat{p}_1|^2$ is robust, and has also been verified in numerical simulations of freely decaying quasi-geostrophic turbulence, the variance of the $|\nabla\chi_1|^2$ term has been found to be dependent both on the details of the forcing and damping (in particular with respect to the vertical dependence of the prescribed $\overline{u}_0(z)$ of the mean baroclinically unstable flow) and also on the depth variation of the stratification parameter S. These results can be *a posteriori* rationalized by examining the right-hand side of the diagnostic equations defining $\hat{p}_1$ and χ_1. We see that the right-hand of (2.4) is completely independent of the existence of a variable stratification S and of a mean streamfunction field such as $\overline{\psi}_0 = -\overline{u}_0(z)y$, while this is not so for the right-hand side of (2.6). Figure 5(*b*)

shows the total variance of $\langle|\gamma_L|^2\rangle/E$ (continuous line), confirming its dominance by the pressure term above $z = -0.3$ (i.e. in the thermocline), and a substantial degree of compensation between the three acceleration components below that level. In this specific simulation, this is caused by the weak stratification value below the thermocline ($z = -0.3$). We have also plotted vertical profiles of the variance of potential vorticity and of kinetic energy on the same graph.

Other numerical simulations performed with different profiles of S have confirmed its preponderant influence on the vertical structure below the thermocline of quantities such as those plotted in figure 5.

4. Conclusion

We have identified the different degrees of freedom for the Lagrangian accelerations for geostrophic turbulence associated, respectively, with the ageostrophic pressure gradient, the divergence potential gradient, and the β-effect term. Numerical simulations have revealed the dominant role played by the ageostrophic pressure component.

For the global statistics in Fourier space, we have documented the steepness of the Lagrangian accelerations horizontal wavenumber spectrum for equilibrium geostrophic turbulence, and confirmed the robustness of the analytical (quasi-normal) estimates. The Lagrangian accelerations display an inertial slope in horizontal wavenumber which is very similar to that of the horizontal velocity field. In frequency space, an important property of the Lagrangian velocity spectrum is its steepness, leading to a preponderant role of the lowest and intermediate frequencies of motion in dispersion and stirring.

The local properties in physical space are governed by the accelerations gradient tensor, whose eigenvalues provide a criterion to partition the flow into regions with different stirring dynamics. This criterion underlines the quantitative importance of the Lagrangian variation of the strain rate along a particle trajectory, in addition to the role played by the instantaneous strain rate stressed by previous studies (e.g. Okubo 1970; Weiss 1991; Mariotti, Legras & Dritschel 1994). Our approach takes into account the short time variations of the flow captured by the acceleration terms and thus amounts to solving the flow evolution equations by a Taylor series, over a short time (Ohkitani & Kishiba 1995). In a given horizontal plane, numerical simulations confirm that the maxima of the positive eigenvalue of the accelerations gradient tensor enable the extrema in the potential vorticity gradient to be located accurately. The vertical distribution of tracer gradients is entirely constrained by the horizontal one, while the reverse is not true so that the three-dimensional distribution of quasi-geostrophic stirring is degenerate. We have made explicit analytically how the tensor $\boldsymbol{M}$ which governs the three-dimensional tracer gradient entirely depends on the three-dimensional Lagrangian accelerations gradient tensor.

The role of the β-effect on the Lagrangian accelerations, besides the usual well-known propagation effects, is to introduce a meridional component in the accelerations; β plays a non-negligible role in the anisotropy of the tracer transport geometry through its influence on the ageostrophic pressure field geometry.

We have not addressed in the present paper regimes of strong intermittency, which would be favoured by smaller β values than the typical midlatitude oceanic regimes reported here. We expect that the analytical considerations of §3 concerning the topology of stirring would still hold in that case. What needs to be assessed quantitatively in the case of strong intermittency is the steepness of both the wavenumber and frequency spectra of Lagrangian accelerations.

Computing ressources were provided by Institut du Développement et des Res sources en Informatique Scientifique. We thank one of the referees for insightful remarks on the manuscript.

Appendix A. Quasi-normal estimate of the ageostrophic pressure wavenumber spectrum

We detail here the formalism leading to the estimate of the spectral characteristics of the ageostrophic pressure $\hat{p}_1$:

$$\nabla^2 \hat{p}_1 = 2J_{xy}(u_0, v_0) + \beta u_0 = -\tfrac{1}{2} W + \beta u_0. \tag{A 1}$$

At a given level z, the covariance function of variable X versus the horizontal lag $\boldsymbol{r}$ is related to its wavenumber spectrum through

$$B_{XX}(\boldsymbol{r}, z) = \frac{1}{2\pi} \int\int \exp^{-\mathrm{i}\boldsymbol{k}\cdot\boldsymbol{r}} S_X(\boldsymbol{k}, z) \mathrm{d}\boldsymbol{k},$$

where $\boldsymbol{k} = (k, \phi)$ and $\boldsymbol{r} = (r, \theta)$ in polar coordinates in Fourier and physical lag space respectively. In the case of $X \equiv \psi_0$, if we retain only the horizontally isotropic contribution of the streamfunction spectrum, we have found that the following analytical shape suitably fits the forced-damped numerical solutions of HH86:

$$kS_{\psi_0}(k, z) = \frac{15E(z)a^3 k}{(a^2 + k^2)^{7/2}}, \tag{A 2}$$

where $E(z)$ is the kinetic energy spectrum at a given vertical level z. Such a choice for S_{ψ_0} corresponds to a k^{-4} kinetic energy spectrum power-law behaviour in the enstrophy inertial range and it implies that the covariance function for ψ_0 is

$$B_{\psi_0\psi_0}(r, z) = \int_0^\infty S_\psi(k) J_0(kr)\, r\mathrm{d}r = 12 \frac{E^2(z)}{Z(z)} \mathrm{e}^{-\tilde{r}} (1 + \tilde{r} + \tfrac{1}{3}\tilde{r}^2),$$

where the relative enstrophy at that same level z is $Z(z) = 4a^2 E(z^{1/2})$ (as implied by (A 2)), and we have introduced the non-dimensional lag $\tilde{r} = \frac{1}{2}(Z/E)\, r$.

We have checked in our numerical simulations that the term involving β on the right-hand side of (A 1) is little correlated with the nonlinear term W, so that the covariance of the Laplacian of $\nabla^2 \hat{p}_1$ versus spatial lag $\boldsymbol{r}$ is well approximated by†

$$B_{\Delta\hat{p}_1 \Delta\hat{p}_1}(\boldsymbol{r}) \approx \tfrac{1}{4} B_{WW}(\boldsymbol{r}) + \beta^2\ B_{u_0 u_0}(\boldsymbol{r}).$$

We have

$$B_{WW}(\boldsymbol{r}) = \left[B_{\sigma^2\sigma^2}(\boldsymbol{r}) + B_{\omega^2\omega^2}(\boldsymbol{r}) - 2B_{\sigma^2\omega^2}(\boldsymbol{r})\right]. \tag{A 3}$$

The quasi-normal evaluation of (A 3) for non-zero lag r yields

$$\begin{aligned} B_{WW}(\boldsymbol{r}) \;=\; & 2\left[B^2_{\sigma_n\sigma_n}(\boldsymbol{r}) + B^2_{\sigma_s\sigma_s}(\boldsymbol{r}) + B^2_{\omega\omega}(\boldsymbol{r}) + 2B^2_{\sigma_n\sigma_s}(\boldsymbol{r}) - 2B^2_{\sigma_n\omega}(\boldsymbol{r}) - 2B^2_{\sigma_s\omega}(\boldsymbol{r})\right] \\ & + B^2_{\sigma_n\sigma_n}(0) + B^2_{\sigma_s\sigma_s}(0) + B^2_{\omega\omega}(0) \\ & + 2B_{\sigma_n\sigma_n}(0)B_{\sigma_s\sigma_s}(0) - 2B_{\sigma_n\sigma_n}(0)B_{\omega\omega}(0) - 2B_{\sigma_s\sigma_s}(0)B_{\omega\omega}(0). \end{aligned}$$

† All quantities are defined at a given level z, but for notational convenience, the z-dependence of the covariance function is omitted in the following.

The spatial homogeneity of the turbulence implies that $\langle\sigma^2\rangle = \langle\omega^2\rangle$. Since the components of strain and vorticity are all mutually statistically orthogonal, the spatial homogeneity moreover yields

$$B_{\sigma_n\sigma_n}(0) = B_{\sigma_s\sigma_s}(0) = \tfrac{1}{2}B_{\omega\omega}(0) = Z,$$

so that

$$B_{WW}(0) = 12Z^2,$$

$$B_{WW}(\boldsymbol{r}) = 2\left[B^2_{\omega\omega}(\boldsymbol{r}) + B^2_{\sigma_n\sigma_n}(\boldsymbol{r}) + B^2_{\sigma_s\sigma_s}(\boldsymbol{r})\right] + B^2_{\sigma_n\sigma_s}(\boldsymbol{r}) - B^2_{\sigma_n\omega}(\boldsymbol{r}) - B^2_{\sigma_s\omega}(\boldsymbol{r}).$$

Using the rotation symmetries in polar coordinates of the operators which are involved in the expression the strain components σ_n, σ_s and in the vorticity ω, yields

$$\begin{aligned}
B_{\omega\omega}(\boldsymbol{r}) &= \int_0^\infty k^4\ S_\psi(k)J_0(kr),\\
B_{\sigma_n\sigma_n}(\boldsymbol{r}) + B_{\sigma_s\sigma_s}(\boldsymbol{r}) &= B_{\omega\omega}(\boldsymbol{r}),\\
B_{\sigma_n\sigma_n}(\boldsymbol{r}) - B_{\sigma_s\sigma_s}(\boldsymbol{r}) &= \frac{1}{2\pi}\int\int \exp^{-\mathrm{i}\boldsymbol{k}\cdot\boldsymbol{r}} k^4\cos(4\phi)S_\psi(k)\mathrm{d}\boldsymbol{k}\\
&= \left[\int_0^\infty k^4\ S_\psi(k)J_4(kr)\right]\cos(4\theta),\\
2B_{\sigma_n\sigma_s}(\boldsymbol{r}) &= \frac{1}{2\pi}\int\int \exp^{-\mathrm{i}\boldsymbol{k}\cdot\boldsymbol{r}} k^4\sin(4\phi)S_\psi(k)\mathrm{d}\boldsymbol{k}\\
&= \left[\int_0^\infty k^4\ S_\psi(k)J_4(kr)\right]\sin(4\theta),\\
B_{\sigma_n\omega}(\boldsymbol{r}) &= \frac{1}{2\pi}\int\int \exp^{-\mathrm{i}\boldsymbol{k}\cdot\boldsymbol{r}} k^4\sin(2\phi)S_\psi(k)\mathrm{d}\boldsymbol{k}\\
&= \left[-\int_0^\infty k^4\ S_\psi(k)J_2(kr)\right]\sin(2\theta),\\
B_{\sigma_s\omega}(\boldsymbol{r}) &= \frac{1}{2\pi}\int\int \exp^{-\mathrm{i}\boldsymbol{k}\cdot\boldsymbol{r}} k^4\cos(2\phi)S_\psi(k)\mathrm{d}\boldsymbol{k}\\
&= \left[-\int_0^\infty k^4\ S_\psi(k)J_2(kr)\right]\cos(2\theta).
\end{aligned}$$

This allows a considerable simplification of the covariance of pressure Laplacian which is exactly isotropic versus spatial lag r:

$$\frac{B_{WW}(r)}{16Z^2} = \left[\tfrac{3}{4}\ \mathscr{F}^2_0(r) + \tfrac{1}{4}\ \mathscr{F}^2_4(r) - \mathscr{F}^2_2(r)\right],$$

denoting by $\mathscr{F}_n$ the transform

$$\mathscr{F}_n(r) = \frac{1}{2Z}\int_0^\infty k^4 S_\psi(k)J_n(kr)\ k\mathrm{d}k, \quad n = 0, 2, 4,$$

where J_n is the Bessel function of order n. This leads to

$$\frac{1}{12Z^2}B_{WW}(\tilde{r}) = \frac{1}{2Z}B_{\omega\omega}(2\tilde{r}), \tag{A 4}$$

with

$$B_{\omega\omega}(\tilde{r}) = 2Z\ \mathrm{e}^{-\tilde{r}}\ (1 - \tfrac{7}{8}\tilde{r} + \tfrac{1}{8}\tilde{r}^2).$$

This relation between the covariance functions of W and ω implies that their spectra verify

$$S_W(k) = \tfrac{3}{2}\, Z(z)\, S_\omega(\tfrac{1}{2}k).$$

The spectra of W and relative vorticity $\omega = \nabla^2\psi_0$ are thus similar in their power-law behaviours, both at small and large scales, the spectral peak of W being at twice that of relative vorticity. Similar results had also been found by Larchevêque (1990) for two-dimensional turbulence, assuming a self-similar inertial-range spectrum. Our results here concern a spectrum shape, which is appropriate for a case of forced-damped turbulence. We note that Larchevêque (1990) has proved that an Eddy-Damped Quasi-Normal Markovian closure yields exactly the same results as a more simple quasi-normal treatment, thereby motivating our choice of the latter.

The spectrum of $\Delta\hat{p}_1$ is therefore

$$S_{\Delta\hat{p}_1}(k) \approx \tfrac{3}{8}\, Z(z)\, S_\omega(\tfrac{1}{2}k) + \beta^2 S_{u_0}(k). \tag{A 5}$$

The spectrum of $\nabla\hat{p}_1$

$$S_{|\nabla\hat{p}_1|}(k) \approx \tfrac{3}{32}\, Z\, S_{|\boldsymbol{u}_0|}(\tfrac{1}{2}k) + \tfrac{1}{2}\beta^2 S_{\psi_0}(k), \tag{A 6}$$

is also similar to that of $|\boldsymbol{u}_0|$, because of the dominance of the first term and its variance is given by

$$\langle|\nabla\hat{p}_1|^2\rangle \approx \left(\tfrac{3}{4}Z(z) + 6\beta^2\frac{E(z)}{Z(z)}\right) E(z). \tag{A 7}$$

Finally, the total spectrum of γ_L is well approximated by

$$S_{|\gamma_L|}(k) \approx \tfrac{3}{32}\, Z\, S_{|\boldsymbol{u}_0|}(\tfrac{1}{2}k) + \tfrac{3}{2}\beta^2 S_{\psi_0}(k). \tag{A 8}$$

REFERENCES

Babiano, A., Basdevant, C., LeRoy, P. & Sadourny, R. 1987 Single particle dispersion, lagrangian structure function and lagrangian energy spectrum in two-dimensional turbulence. *J. Mar. Res.* **45**, 107–131.

Babiano, A., Basdevant, C. & Sadourny, R. 1985 Structure functions and dispersion laws in two-dimensional turbulence. *J. Atmos. Sci.* **42**, 107–131.

Bartello, P. & Holloway, G. 1991 Passive scalar transport in β-plane turbulence. *J. Fluid Mech.* **223**, 521–536.

Basdevant, C. & Philipovitch, T. 1994 On the validity of the "Weiss criterion" in two-dimensional turbulence. *Physica* D **73**, 17–30.

Batchelor, G. K. 1951 Pressure fluctuation in isotropic turbulence. *Proc. Camb. Phil. Soc.* **47**, 359–374.

Benzi, R., Patarnello, S. & Santangelo, P. 1988 Self-similar coherent structures in two-dimensional decaying turbulence. *J. Phys.* A: *Math. Gen.* **21**, 1221–1237.

Borgas, M. S. & Sawford, B. L. 1991 The small-scale structure of acceleration correlations and its role in the statistical theory of turbulent dispersion. *J. Fluid Mech.* **228**, 295–320.

Bowman, K. P. & Chen, P. 1994 Mixing by barotropic instability in a nonlinear model. *J. Atmos. Sci.* **51**, 3692–3705.

Brachet, M., Meneguzzi, M., Politano, H. & Sulem, P. 1988 The dynamics of freely decaying two-dimensional turbulence. *J. Fluid Mech.* **194**, 333–349.

Charney, J. 1971 Geostrophic turbulence. *J. Atmos. Sci.* **28**, 1087–1095.

Cho, J. Y. K. & Polvani, L. M. 1996 The emergence of jets and vortices in freely evolving, shallow-water turbulence on a sphere. *Phys. Fluids* **8**, 1531–1552.

Chong, M. S., Perry, A. E. & Cantwell, B. J. 1990 A general classification of three-dimensional fields. *Phys. Fluids* A **2**, 765–777.

Davies-Jones, R. 1991 The frontogenetical forcing of secondary circulations. Part I: the duality and generalization of the Q vector. *J. Atmos. Sci.* **48**, 497–509.

Elhmaïdi, D., Provenzale, A. & Babiano, A. 1994 Elementary topology of two-dimensional turbulence from a Lagrangian viewpoint. Part 1. Single particle dispersion. *J. Fluid Mech.* **257**, 533–558.

Haynes, P. & Anglade, J. 1997 The vertical-scale cascade in atmospheric tracers due to large-scale differential advection. *J. Atmos. Sci.* **54**, 1121–1136.

Herring, J. 1980 Statistical theory of quasiqeostrophic turbulence. *J. Atmos. Sci.* **37**, 969–977.

Holloway, G. 1986 Eddies, waves, circulation, and mixing: statistical geofluid mechanics. *Ann. Rev. Fluid Mech.* **18**, 91–147.

Holzer, M. & Siggia, E. 1993 Skewed, exponential pressure distributions for Gaussian velocities. *Phys. Fluids* A **5**, 2525–2532.

Hoskins, B. J., Draghici, I. & Davies, H. C. 1978 A new look at the ω-equation. *Q. J. R. Met. Soc.* **104**, 31–38.

Hua, B. L. 1994 Skewness of the generalized centrifugal force divergence for a joint normal distribution of strain and vorticity components. *Phys. Fluids* A **6**, 3200.

Hua, B. L. & Haidvogel, D. 1986 Numerical simulations of the vertical structure of quasigeostrophic turbulence. *J. Atmos. Sci.* **43**, 2923–2936 (referred to here in as HH86).

Hua, B. L. & Klein, P. 1998 An exact criterion for the stirring properties of nearly two-dimensional turbulence. *Physica* D **113**, 98–110.

Klein, P., Tréguier, A. M. & Hua, B. L. 1998 Quasiqeostrophic stirring of thermohaline fronts. *J. Mar. Res.* in press.

Kundu, P. K. 1990 *Fluid Mechanics.* Academic.

Larchevêque, M. 1990 Pressure fluctuations and lagrangian accelerations in two-dimensional Incompressible isotropic turbulence. *Eur. J. Mech.* B *Fluids* **9**, 109–128.

Lighthill, J. 1978 *Waves in Fluids.* Cambridge University Press.

Maltrud, M. E. & Vallis, G. K. 1991 Energy spectra and coherent structures in forced two-dimensional and beta-plane turbulence. *J. Fluid Mech.* **228**, 321–342.

Mariotti, A., Legras, B. & Dritschel, D. G. 1994 Vortex stripping and the erosion of coherent structures in two-dimensional flow. *Phys. Fluids* A **6**, 3954–3962.

McIntyre, M. E. 1989 On the Antarctic Ozone Hole. *J. Atmos. Terr. Phys.* **51**, 29–43.

McWilliams, J. C. 1984 The emergence of isolated, coherent vortices in turbulent flow. *J. Fluid Mech.* **146**, 21–43.

McWilliams, J. C. 1989 Statistical properties of decaying geostrophic turbulence. *J. Fluid Mech.* **198**, 199–230.

McWilliams, J. C., Owens, W. B. & Hua, B. L. 1986 An objective analysis of the POLYMODE Local Dynamics Experiment. I- General formalism. *J. Phys. Oceanogr.* **16**, 506–522.

McWilliams, J. C., Weiss, J. B. & Yavneh, I. 1994 Anisotropy and coherent vortex structures in planetary turbulence. *Science* **264**, 410–413

Ohkitani, K. & Kishiba, S. 1995 Nonlocal nature of vortex stretching in an inviscid fluid. *Phys. Fluids* A **7**, 411–421.

Okubo, A. 1970 Horizontal dispersion of floatable particles in the vicinity of velocity singularities such as convergences. *Deep-Sea Res.* **17**, 445–454.

Panetta, R. L. 1993 Zonal jets in wide baroclinically unstable regions: persistence and scale selection. *J. Atmos. Sci.* **50**, 2073–2106.

Pedlosky, J. 1987 *Geophysical Fluid Dynamics,* Springer.

Pierrehumbert, R. T. & Yang, H. 1993 Global chaotic mixing on isentropic surfaces. *J. Atmos. Sci.* **50**, 2462–2480.

Polvani, L. M., McWilliams, J. C., Spall, M. A. & Ford R. 1994 The coherent structures of shallow-water turbulence: deformation-radius effects, cyclone/anticyclone asymmetry and gravity-wave generation. *Chaos* **4**, 177–186.

Rhines, P. B. 1979 Geostrophic turbulence. *Ann. Rev. Fluid Mech.* **11**, 401–411.

Rhines, P. B. 1975 Waves and turbulence on a beta-plane. *J. Fluid Mech.* **69**, 417–443.

Rupolo, V., Hua, B. L., Provenzale, A. & Artale, V. 1996 Lagrangian velocity spectra at 700 m in the Western North Atlantic. *J. Phys. Oceanogr.* **26**, 1591–1607.

Taylor, G. I. 1921 Diffusion by continuous movements. *Proc. Lond. Math. Soc.* **20**, 196–211.

Taylor, G. I. 1935 Statistical theory of turbulence. IV Diffusion in a turbulent air stream. *Proc. R. Soc. Lond.* A **151**, 465–478.

Weiss, J. 1991 The dynamics of enstrophy transfer in two-dimensional hydrodynamics. *Physica* D **48**, 273–294.

Xu, Q. 1992 Ageostrophic pseudo-vorticity and geostrophic *C*-vector forcing – A new look at the *Q* vector in three dimensions. *J. Atmos. Sci.* **49**, 981–990.